Correlating Ionic Conductivity, Oxygen Transport and ORR with Structure of Dialkylacetamide-Based Electrolytes for Lithium-Air Batteries

Amell Alsudairi,[1,2,*] Amal Lajami,[1] Ian Kendrick,[1] Sanjeev Mukerjee,[1,] and K. M. Abraham [1,***,z]**

[1]*Northeastern University Center for Renewable Energy Technology, Department of Chemistry and Chemical Biology, Northeastern University, Boston, Massachusetts 02115, USA*
[2]*Chemistry Department, Faculty of Science, King Abdulaziz University, Jeddah 21589, Saudi Arabia*

Chemical structures of lithium and tetrabutylammonium (TBA) salt solutions in N,N-dimethylacetamide (DMAc) and N,N-diethylacetamide (DEAc), two high Donor Number organic solvents, have been studied. In LiX salt solutions (where X = PF_6^-, $CF_3SO_3^-$, ClO_4^- and NO_3^-), solvation occurs when the Li^+ bonds with the solvent's carbonyl group forming $Li^+[O{=}C(CH_3)N(CH_3)_2]_nX^-$ ion pairs. Infrared and ^{13}C-NMR spectra are consistent with the ion pair being solvent-separated when the anion is PF_6^-, ClO_4^- or NO_3^-, and a contact ion pair in the case of $CF_3SO_3^-$. Chemical interactions between TBA^+ and the solvents to form conducting solutions appeared to be dipolar in nature. Ionic conductivities of TBA^+ and Li^+ electrolytes were measured and correlated with their viscosities. In 0.1M $TBAPF_6$/DMAc, the O_2 solubility and diffusion coefficient (3.09×10^{-6} mol/cm^{-3} and 5.09×10^{-5} cm^{2}s^{-1}, respectively) measured using microelectrode technique are typical of values measured in several TBA^+ solutions. Microelectrode voltammetry revealed steady-state limiting current behavior for oxygen reduction reactions (ORR) in TBAX/DMAc electrolytes indicating a reversible ORR process. Conversely, microelectrode current-voltage data for ORR in LiX/DMAc electrolytes revealed irreversible behavior mainly ascribed to the blockage of the electrode surface by insoluble ORR products. The ORR in DMAc correlated with its high Donor Number and the overall process conformed to the Hard-Soft Acid-Base theory.

Manuscript submitted November 1, 2018; revised manuscript received January 14, 2019. Published January 29, 2019. This was Paper 365 presented at the Cancun, Mexico, Meeting of the Society, September 30–October 4, 2018.

An in-depth understanding of the chemistry behind oxygen reduction reactions (ORR) in non-aqueous electrolytes is essential to improve the discharge performance and rechargeability of Lithium-air (Li-air) batteries. We have satisfactorily explained the effect of different non-aqueous organic solvents on the oxygen redox chemistry using the Hard-Soft Acid-Base (HSAB) theory[1–3] which states that soft Lewis acids prefer to combine with soft Lewis bases while hard Lewis acids prefer to bond with hard Lewis bases to form acid-base complexes. The reduction products of O_2 have a range of Lewis basicity from the soft base superoxide (O_2^-) to the hard bases peroxide (O_2^{2-}) and monoxide (O^{2-}). In organic solvent-based electrolytes the metal salt cations are solvated by the electron donor solvents which in turn modulates the Lewis acidity of the cations. Thus, although Li^+ is a strong Lewis acid it acquires softer acid characteristics depending upon the basicity of the solvents with which it forms solvates, formulated as ((solvent)$_n$ Li^+) where n is typically four.[4–7] Electron donor solvents with High Gutman Donor Numbers (DN) are strong Lewis bases which through solvation make Li^+ a softer Lewis acid leading to stronger interaction between the solvated Li^+, (solvent)$_n$ Li^+, and the weak Lewis base superoxide anions (O_2^-) formed as the one-electron reduction product of O_2 in organic electrolytes.[3] Low Donor Number solvents modulates the Lewis acidity of Li^+ to a lesser extent that it maintains its hard acidity to stabilize the hard basses O_2^{2-} and O^{2-} formed from O_2 reduction. The HSAB theory satisfactorily explained the ORR behavior in different solvents used in the non-aqueous rechargeable Lithium-air battery. For example, the organic ethers such as dimethoxy ethane (DME) (DN = 20) and tetraethyleneglycol dimethyl ether (TEGDME) (DN = 16.6) having relatively high chemical stability toward the Li metal anode are low Donor Number solvents whereas dimethyl sulfoxide (DMSO) (DN = 29.8) and *N,N*-dimethyl acetamide ($(CH_3)_2NCOCH_3$, DMAc) (DN = 27.8) are high donor number solvents.[8]

The effects of Li^+ solvation on the ORR mechanism in non-aqueous solutions have been investigated by different research groups.[5,9–23] Johnson et al. have compared this effect in four different solvents with varying DNs (DMSO, acetonitrile (ACN), DME and 1-methlimidazole(Me-Im)).[15] Their study, built upon previous studies of solvent effects on ORR,[1–3] lead them to conclude that during the ORR, the Li_2O_2 can form in one of two pathways: the surface mechanism and the solution mechanism. The surface mechanism takes place in low DN solvents where the O_2 is reduced to superoxide on the electrode surface and due to the weak solvation, the Li^+ ion reacts with the surface superoxide forming surface adsorbed LiO_2 which successively undergoes further reduction to form Li_2O_2 on the surface. On the other hand, the solution mechanism takes place in high DN solvents. In this case, due to its strong solvation by the solvent molecules, Li^+ is not available to combine with the surface superoxide radical on the electrode surface. Consequently, the superoxide radical diffuses to the solution where the formation of soluble LiO_2 takes place and successively reduces to form the Li_2O_2.[15] The formation of $LiO_{2(ads)}$ and $LiO_{2(sol)}$ and its relation with the DN of the solvent was further investigated and supported by other research groups.[5,21,23,24] The effect of the DN of the lithium salt's anion has been investigated as well. In low DN solvents, the DN of the salt affects the mechanism of the ORR. If the DN of both the solvent and the anion is low, the surface mechanism takes place (due to weak solvation between the Li^+ and the anion) leading to the formation of a thin compact film of Li_2O_2 on the electrode surface. On the contrary, if the solvent's DN is low and the anion's DN is high (such as NO_3^-), the anion solvates the lithium ion strongly leading to a solution mechanism where the superoxide ion diffuses away from the surface leading to the formation of $LiO_{2(sol)}$ which disproportionate forming Li_2O_2.[9,10,14,16,18] On the other hand, in high DN solvents, the DN of the anion does not change the ORR mechanism pathway due to the strong solvation between the solvent molecules and the lithium ion.[9,10,18]

Walker et al.[25] reported the operation of a Li-O_2 battery using DMAc-based electrolyte. Even though Lithium metal reacts with DMAc, they stabilized the Li anode by modifying the solid-electrolyte interphase (SEI) on the Li anode with the use of lithium nitrate salt in the electrolyte.[25–27] The results of Walker et al. have encouraged

*Electrochemical Society Student Member.
**Electrochemical Society Member.
***Electrochemical Society Fellow.
[z]E-mail: kmabraham@comcast.net

us to perform a detailed study of the structure-property relationships of Li^+-conducting electrolytes in DMAc and diethylacetamide ($(C_2H_5)_2NCOC_2H_5$, DEAc) (DN = 32) and to correlate the data with O_2 transport properties and electrochemistry in these electrolytes. Our previous study of the use of DMAc as a thermally stable solvent for use in a rechargeable sodium battery operating in the 100–125°C range further served as an impetus for this investigation on the usefulness of DMAc and DEAc as electrolyte solvents in the non-aqueous Li-air battery.[28] A particular emphasis in this study is the use of microelectrodes for O_2 transport property measurements and ORR studies.

In this paper, we report a detailed study of the ORR in DMAc electrolytes prepared using a number of tetrabutylammonium (TBA^+) and lithium (Li^+) salts including $TBAPF_6$, $LiPF_6$, $TBACF_3SO_3$, $LiCF_3SO_3$, $TBAClO_4$, $LiClO_4$, $TBANO_3$ and $LiNO_3$. For comparison, *N,N*-diethyl acetamide (DEAc) (DN = 32) was studied as well with selected salts. Electrochemical results obtained with microelectrodes are discussed in light of those obtained using traditional macroelectrodes to distinguish between the influence of kinetic factors and O_2 mass transport on ORR in these electrolytes. In addition, the results obtained in dialkylacetamides are compared to those previously obtained in electrolytes prepared with the same salts in the high Donor Number solvent DMSO.[12] We thus present a comprehensive picture of the influence of solvent electron donor properties on ORR in electrolytes prepared in high Donor Number solvents. We believe that studying the O_2 transport properties and the ORR in dialkylacetamide-based electrolytes can contribute to a better understanding of the ORR process in Li-air batteries.

Experimental

Materials.—Tetrabutylammonium (TBA) salts (tetrabutylammonium hexafluorophosphate, tetrabutylammonium trofluoromethanesulphonate, tetrabutylammonium perchlorate and tetrabutylammonium nitrate) and lithium salts (lithium hexafluorophosphate, lithium trifluoromathane sulfonate, lithium perchlorate and lithium nitrate) as well as the solvents anhydrous dimethyl acetamide (DMAc) and anhydrous dimethyl sulfoxide (DMSO) purchased from Sigma Aldrich were used as received. The diethyl acetamide (DEAc) purchased from Alfa Aesar was dried over 3 Angtsrom molecular sieves (from Sigma Aldrich) by storing about 30 grams molecular sieves in 250 ml of the solvent for a period of 5 days. The lithium foil and the silver wires were both purchased from Alfa Aesar as well. All chemicals were stored in the Argon atmosphere of an M-Braun glove box maintained with less than 1 ppm humidity level.

Measurement of electrolyte properties.—Ubbleohde Viscometer (C-545) was used to measure the kinematic viscosities of the electrolytes at 25°C while a Thermo-Orion conductivity cell was used to measure the conductivities of the electrolytes over the temperature range of −20 to 40°C. An ESPEC Environmental chamber was used to maintain the temperature of the conductivity cell. Bruker ATR Infra-Red spectrometer was used to record the FT-IR spectra of solvents, electrolyte solutions and salts. A 500MHz Varian Inova NMR spectrometer was used to acquire ^{13}C-NMR spectra for the solvents and electrolyte solutions, mixed with deuterated benzene (0.03% (v/v) TMS), which were freshly made and sealed in an argon atmosphere glove box. The ^{13}C chemical shifts are reported with respect to the ^{13}C shift of internal TMS (tetramethysilane) reference. All ^{15}N direct observe NMR spectra were recorded on a Bruker 400MHz AVANCE *II* NMR spectrometer at 300K using a multinuclear broadband BBFO probe. Samples were always freshly made and sealed in NMR tubes in an argon atmosphere glove box. Due to the expected long T_1, a 30-degree pulse was used along with a 10s relaxation delay. Proton decoupling was applied during the acquisition period. The ^{15}N chemical shifts are reported with respect to an external sample of 1M $^{15}NH_4Cl$ in 90%H_2O/10%D_2O.

Electrochemistry.—The electrochemical cell used for this study was comprised of a three-electrode cell contained in a beaker with a platinum mesh counter electrode and a $Ag/AgNO_3$ reference electrode while the working electrode was either a planar glassy carbon macroelectrode (0.59 cm diameter) or an 11μm diameter carbon microelectrode. The reference electrode was constructed by immersing a silver wire in a glass tube with a porous tip containing 10 mM $AgNO_3$ with 0.1 M $TBAPF_6$ in DMSO or DMAc.[29] The value of the reference electrode potential with respect to Li/Li^+ was obtained by measuring the potential difference between the Ag/Ag^+ electrode and a clean Li foil immersed in the same electrolyte for a short time. In the case of $Ag/AgNO_3$/DMSO, this value in all DMSO electrolytes was found to be 3.63V while in the case of $Ag/AgNO_3$/DMAc, it was 3.72V in all DMAc electrolytes. In the case of DEAc, a Ag/AgO was used as the reference electrode. It was prepared by immersing a clean and polished silver wire in a concentrated nitric acid for 30 minutes then it was washed with MilliQ water. By then a white layer of silver oxide was formed on the silver wire's surface. The Ag/AgO potential with respect to Li/Li^+ in DEAc electrolytes was found to be 3.09V.

Cyclic voltammetry measurements were obtained in TBA^+- based and Li^+- based electrolytes using either the carbon microelectrode or the glassy carbon microelectrodes at different scan rates while potential step chronoamperometry was performed in TBA^+- based electrolytes using the carbon microelectrodes. All electrochemical experiments were performed inside an Ar-filled glove box where the moisture level was less than 1 ppm.

Results and Discussion

We first discuss the chemical structure of the electrolytes prepared in solutions of Li^+ and TBA^+ salts in DMAc and DEAc. These dialkylacetamide solvents, $CH_3CON(R')_2$ where R' is $-CH_3$ or $-C_2H_5$, each possessing –C=O: and -N: moieties, can potentially act as a bidentate or a monodentate ligand toward Li^+ forming solvates of the general formulas $(solvent)_nLi^+$ or $(solvent)_{n/2}Li^+$ in which n is usually 4. Moreover, when acting as a monodentate ligand, solvent co-ordination to Li^+ can occur either through the oxygen of –C=O: or the nitrogen of –N:. Therefore, it is important to establish the exact structure of Li^+ solvates formed in these electrolytes. The structural information obtained from IR and ^{13}C NMR spectral studies of these electrolytes has allowed us to rationally analyze ion conductivity, oxygen transport and ORR mechanism in these solutions.

Electrolyte structure.—*Ion pair formation.*—Dissolution and solvation of conducting salts in organic solvents results in the formation of ion pairs. They can be contact ion pairs, solvent separated ion pairs or ion aggregates. According to previous studies, in high DN solvents, the DN of the counter anions does not change the ORR mechanism (solvent assisted).[9,10,18] This mechanism occurs due to strong solvation between the solvent molecules and the Li^+ leading to the formation of solvent separated ion pairs. According to Bruke et al., in DMSO solutions (high DN) the counter anions does not coordinate with the Li^+.[9,10] However, there are studies that show coordination between anions such as $CF_3SO_3^-$ [triflate] and $(CF_3SO_2)_2N^-$ (bis(trifluoromethanesulfonyl)imide) [TFSI] with the Li^+ (forming contact ion pairs) even in high DN solvents (i.e. DMSO).[12,19]

FT-IR and NMR experiments were conducted in order to confirm the ion pair structure of different Li^+ salts in DMAc solutions. FT-IR spectra for solutions of $LiPF_6$, $LiCF_3SO_3$ and $LiNO_3$ in DMAc recorded to identify the nature of the interaction between the salt and the solvent are shown in Figure 1. As the concentration of the lithium salts increased, the symmetric stretching of carbonyl group in of DMAc shifted to lower wavenumbers from its value at 1641cm^{-1} in the neat solvent. This shift was more pronounced in the case of $CF_3SO_3^-$ (triflate) than in solutions of other salts indicating indicating stronger coordination between the C=O of DMAc and the Li^+ in the triflate. A similar trend was observed in the DEAc solutions, but the shift was larger suggesting stronger solvation between Li^+ and C=O of DEAc. This trend is consistent with the fact that DEAc is a slightly stronger electron donor (higher donor number) than DMAc. Since the dialkylacetamide solvents investigated are tertiary amides,

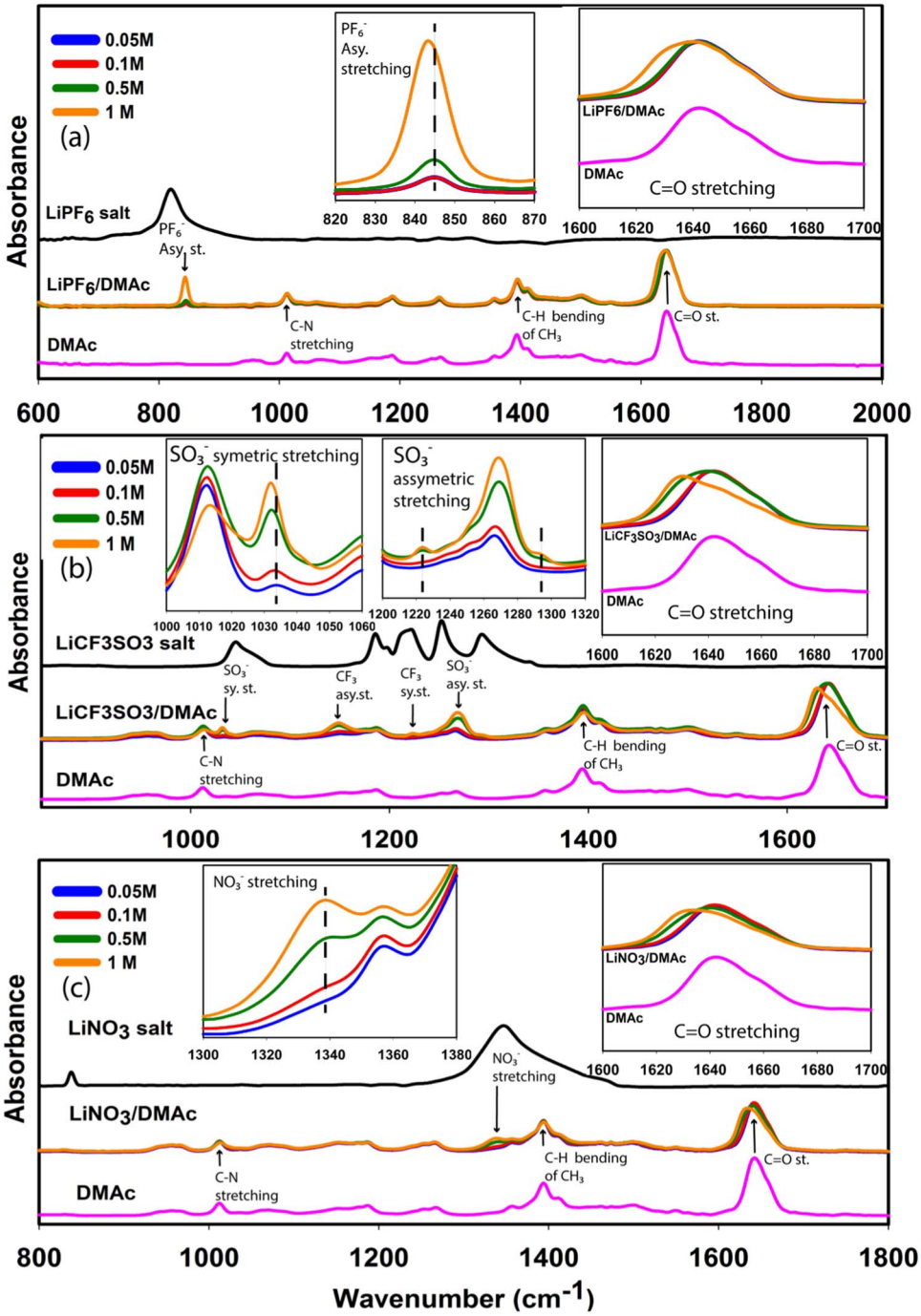

Figure 1. FT-IR spectra of (a) $LiPF_6$ in DMAc solution, (b) $LiCF_3SO_3$ in DMAc solution and (c) $LiNO_3$ in DMAc solution.

FTIR does not show any amide IR peaks making it impossible to determine whether there is co-ordination between the nitrogen and Li^+.

In solutions of $LiCF_3SO_3$, the asymmetric stretching vibrations (ν_{as}) of free triflate ion, at 1270 cm^{-1},[12,13,30,31] split into two peaks (appears slightly above and below the ν_{as} of the free ion) with their intensities increasing as the concentration of triflate ions ($CF_3SO_3^-$) increased. This indicates that the triflate ions are coordinating directly with the small cation Li^+.[12,13,31,32] Additionally, the symmetric stretching vibrations (ν_{ss}) of free triflate ions (at 1031 cm^{-1})[12,13,30–32] has shifted toward lower frequencies as the triflate ion concentration increased, which indicates the formation of an ion pair between the triflate's $S\text{-}O^-$ group and the Li^+[12,31] (see Figure 1b insets). In PF_6^- case, no shift was observed in the PF_6^- asymmetric stretching peak except at a high concentration (1M) (see Figure 1a inset). On the other hand, we have not seen any shifts in the NO_3^- stretching peak (see Figure 1c inset). These observations lead us to conclude that the ion pairs formed between the dimethylacetamide and the salts are solvent-separated when the anion is NO_3^- (high DN) or at concentrations less than 1M of PF_6^- (low DN).[33] This conclusion supports Bruke et al.'s suggestion that the counter anions does not coordinate with the Li^+ when the DN of the solvent is high.[9,10,15] On the other hand, the shift in PF_6^- asymmetric stretching at the high concentration of PF_6^- suggests the formation of a contact ion pair in this case. Also, the shifts in the triflate's symmetric and asymmetric stretching of SO_3^- suggests contact ion pairs when the anion is $CF_3SO_3^-$, in agreement with previous studies in DMSO solutions.[12,19] The formation of the contact

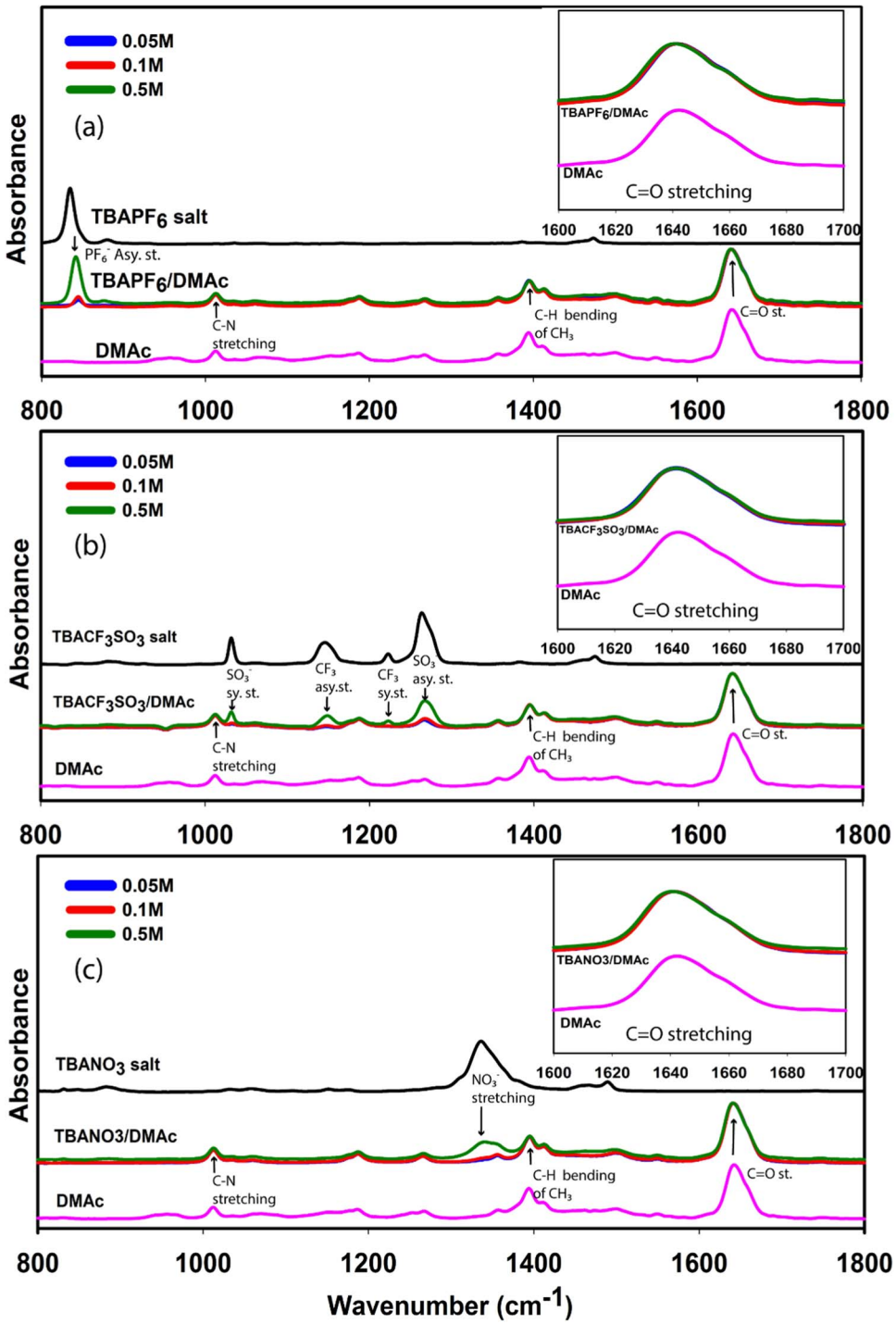

Figure 2. FT-IR spectra of (a) $TBAPF_6$ in DMAc solution, (b) $TBACF_3SO_3$ in DMAc solution and (c) $TBANO_3$ in DMAc solution.

ion pair between the triflate and the Li^+ along with the solvation of Li^+ of by DMAc explains the stronger interaction between DMAc's C=O and the Li^+. When one DMAc (DN=27.8) molecule in the Li^+-solvate is replaced by a triflate anion (DN≈20),[33] the coordination of the three remaining DMAc molecules with Li^+ becomes stronger.

The FT-IR spectra for TBA^+ salts showed no shift in the carbonyl stretching band except for a very minimal shift at high concentrations in both DMAc (Figure 2) and DEAc. This behavior suggests that the TBA^+ ion is weakly solvated in DMAc and DEAc without donor-acceptor bonds. This behavior is similar to what we observed previously for Li^+ and TBA^+ ions in DMSO (another high Donor Number solvent).[12] The lack of point charge co-ordination between TBA^+ and these high DN solvents is consistent with TBA^+ being a soft acid.[1] The fact that TBA salts dissolve in these dialkylacetamides to form conducting electrolytes (Table S1) suggests that there are strong electrostatic interactions between these solvents and the TBA^+ salts. The solvation of Li^+ by the dialkylacetamides provides strong support to the modulation of the Lewis acidity of Li^+ by the high DN solvents such as the amides and sulfoxides.[1–3]

To gain further insights into the interaction between Li salts and the dialkylacetamides, especially to determine if the Nitrogen atom contributes to the solvation of the Li^+, ^{13}C-NMR spectroscopy was

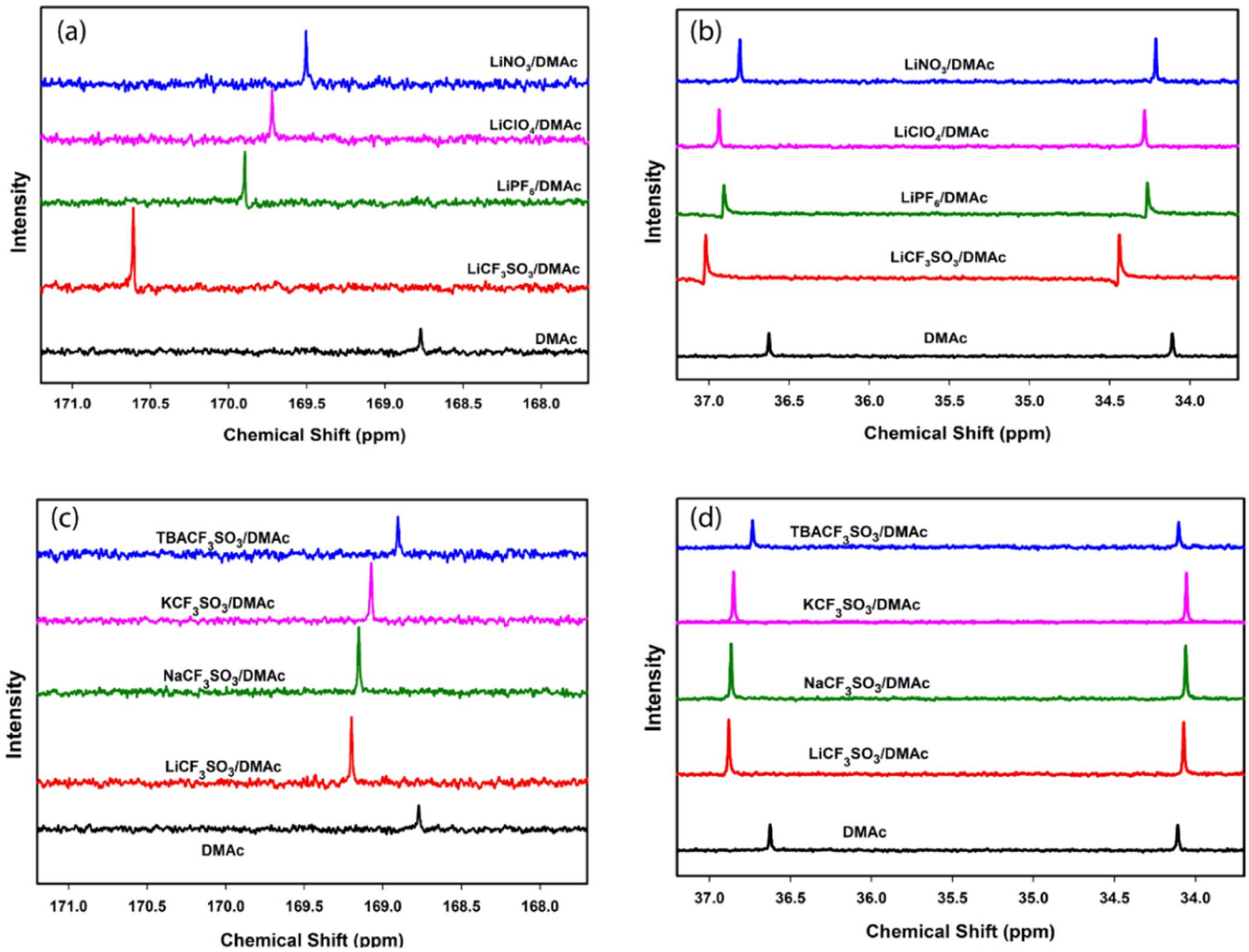

Figure 3. ^{13}C-NMR chemical shift of (a) carbonyl carbon and (b) -N$(CH_3)_2$ carbons for neat DMAc and 1M Li^+ salts solutions in DMAc, (c) carbonyl carbon and (d) -N$(CH_3)_2$ carbons for neat DMAc and 0.5M $CF_3SO_3^-$ salts solutions in DMAc with different cations.

used. When the ^{13}C-NMR spectra of the various lithium salt solutions in DMAc are compared, a positive chemical shift in the ^{13}C peak of DMAc's carbonyl carbon (–C=O) was noticed in all solutions (Figure 3 and Table S2) compared to that in the neat DMAc solvent. This confirms that the DMAc co-ordinates with Li^+ salts through –C=O. The chemical shift in the $CF_3SO_3^-$ solution was much larger than the shifts in the PF_6^-, ClO_4^- and NO_3^- electrolytes (Figure 3a) which again indicates stronger solvation between this salt and DMAc. We notice here that this shift follows the increase in the molecular weight (size of the anion) (Mwt: $NO_3^- < ClO_4^- < PF_6^- < CF_3SO_3^-$) not the DN of the anion (DN: $PF_6^- < ClO_4^- < CF_3SO_3^- < NO_3^-$). Small chemical shifts in the ^{13}C peaks of the N$(CH_3)_2$ methyl carbons were noticed but one of the N-CH_3 carbon peaks was shifted slightly more than the other (Figure 3b), probably due to steric asymmetry. Since the N$(CH_3)_2$ chemical shift is small and not uniform it implies that the nitrogen atom does not interact with Li^+ directly and the noticed shift is caused by the indirect change of electron density on the nitrogen atom due to the interaction between the C=O and Li^+. To confirm this, we recorded ^{15}N-NMR spectra for neat DMAc, $LiPF_6$/DMAc and $LiCF_3SO_3$/DMAc solutions. The neat DMAc's ^{15}N-NMR spectra showed one nitrogen peak at 137.29 ppm and there was no shift in this peak with the addition of either $LiPF_6$ or $LiCF_3SO_3$ (Figure 4).

Cation effect on the ^{13}C Shift was also studied using different triflate salt solutions in DMAc where a shift was in the DMAc's carbonyl carbon was recorded in all solutions. The ^{13}C-NMR chemical shift in the carbonyl carbon was the highest in the case of Li^+ and the lowest in the case of TBA^+ following the order of the cation's Lewis acidity ($Li^+ > Na^+ > K^+ > TBA^+$) (Figure 3c) indicating a stronger co-ordination bond between the cation and the –C=O of DMAc in the case of the stronger Lewis acids than the weaker ones. These findings are in good agreement with our previous studies in propylene carbonate based electrolytes.[1] Again the ^{13}C shift of the carbons attached to the nitrogen atom was very small (Figure 3d). Cation effect was also studied in the case of DEAc solvent using two triflate salts. Similar to DMAc case, the carbonyl carbon's ^{13}C chemical shift was larger in the case of Li^+ than TBA^+ (Table S2).

In the ^{13}C spectrum of a solution of $LiPF_6$ in a 50:50 mixture (volume ratio) of DMAc and DME (1,2-dimethoxyethane, DN = 20), we observed a chemical shift in the DMAc's carbonyl carbon peak (Figure S1(a)) while almost no shift was noticed for the ether carbons (Figure S1(b), (c)). This indicates that the ether solvent is not competing with the amide to solvate the lithium ion in this mixed solvent electrolyte. These results strongly support the contribution of high Donor Number solvents to solvate Li^+ and modulate its Lewis acidity.[2,3,8,12]

The FTIR and NMR results lead us to unambiguously conclude that the dialkylacetamides solvates the lithium salts by forming a monodentate bond with Li^+ through the carbonyl oxygen. The solvates most probably exist as solvent separated ion pairs in $LiNO_3$, $LiClO_4$ and low concentrations of $LiPF_6$ solutions and as contact ion pairs

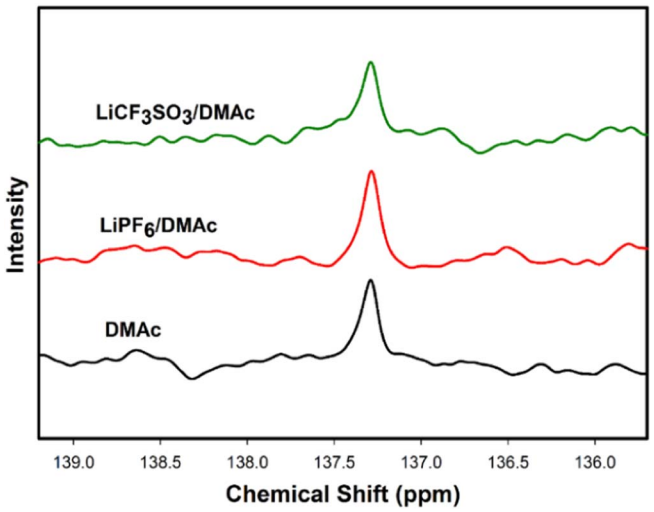

Figure 4. ^{15}N-NMR chemical shift for neat DMAc, 1M $LiPF_6$ in DMAc and 1M $LiCF_3SO_3$ in DMAc.

in the $CF_3SO_3^-$ electrolyte and high concentrations of $LiPF_6$. Based on the NMR and IR data and the well-established fact that Li^+ forms four co-ordinate complexes[4–7] with the electron donor molecules we have drawn the possible structures of the adducts (solvates) formed between the Li^+ salts and DMAc (taking into account that $LiPF_6$ concentration used for our study is low) as shown in Scheme 1.

Due to the solvation of Li^+, its Lewis acidity hardness is modulated in proportion to the basicity (Donor number) of the solvent making it a softer Lewis acid in the lithium salt solutions. As a result, it interacts strongly with the Lewis base superoxide (O_2^-) (softest Lewis base among the O_2 reduction products) formed in ORR in electrolytes prepared from high donor number solvents such as DMAc. In $LiCF_3SO_3$ solutions, one of the Li^+ solvating DMAc molecules is replaced by a triflate ion (higher molecular weight than DMAc). Hence the Li^+ hardness is lowered even more and as a result the Li^+ forms an even more stable ion pair with O_2^- in this solution.

In the supplementary section we used Drago's equation (S2) to calculate the approximate value of enthalpy of formation for the 1:1 adduct between Li^+ and DMAc (47. 4 kcal/mole). This value is comparable to that of DMSO (46 kcal/mole).[12]

Electrolyte conductivity of lithium and TBA salts in dialkylacetamides.—Conductivity and viscosity were measured for electrolytes prepared with Li^+ and TBA^+ conducting electrolytes in DMAc. For comparison we also measured these values for Li^+ and TBA^+ hexafluorophosphate electrolytes in DMSO (Table S1). DMAc itself exhibits lower viscosity than DMSO and, consequently, all DMAc electrolytes have lower viscosities than DMSO electrolytes as well. The relationship between the conductivity, viscosity and concentration is shown in figure S2 in the supplementary section.

The collected conductivity data at different temperatures (range of −20 to 40°C) were fitted to the Arrhenius Equation 1.

$$\text{Log}\,\sigma = \text{Log}\,A - E_a/RT \qquad [1]$$

In Equation 1, σ is conductivity, E_a is the activation energy for conduction, R is the gas constant (8.314 $JK^{-1}mol^{-1}$) and T is the absolute temperature. The resulting plots depicted in Figure 5a showed a less than ideal nonlinear profile of conductivity versus the inverse of temperature. A better fit to Arrhenius behavior is obtained if the conductivity-temperature plot is limited to a narrower temperature range by omitting the values at very low and very high temperatures. An activation energy for conduction was calculated from the resulting conductivity versus the inverse of temperature plot. These values for the DMAc-based electrolytes are shown in Table S2.

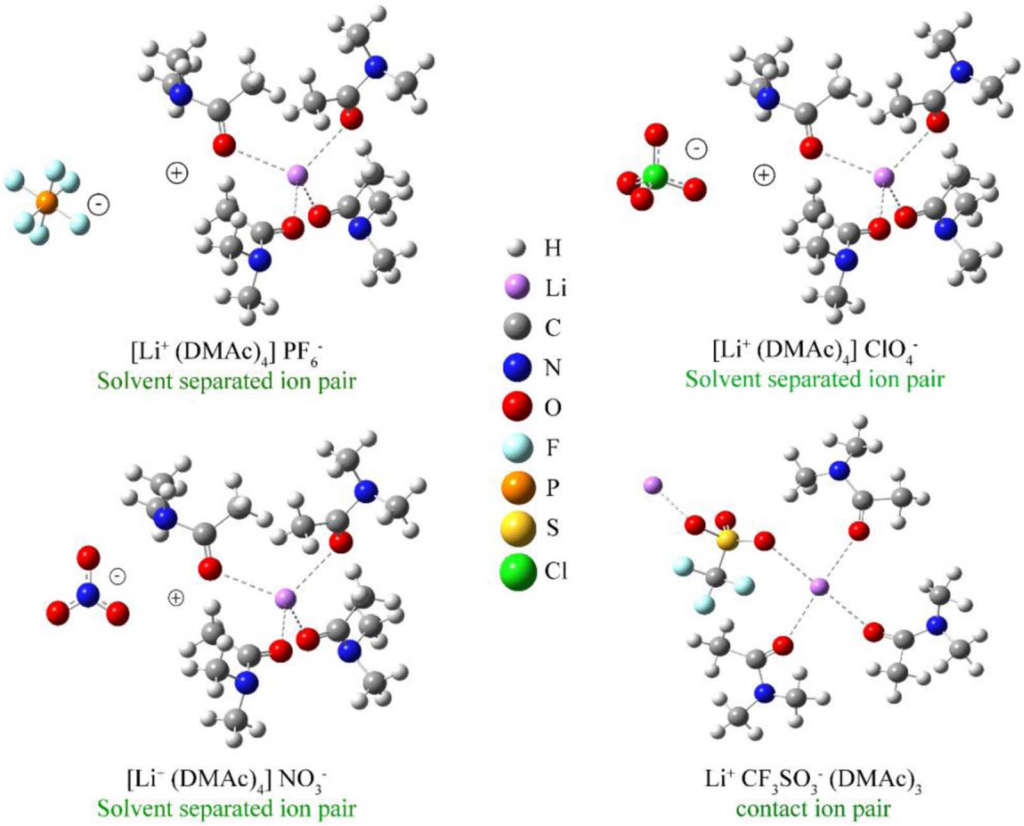

Scheme 1. Possible structures of the adducts (solvates) formed between the Li salts and DMAc.

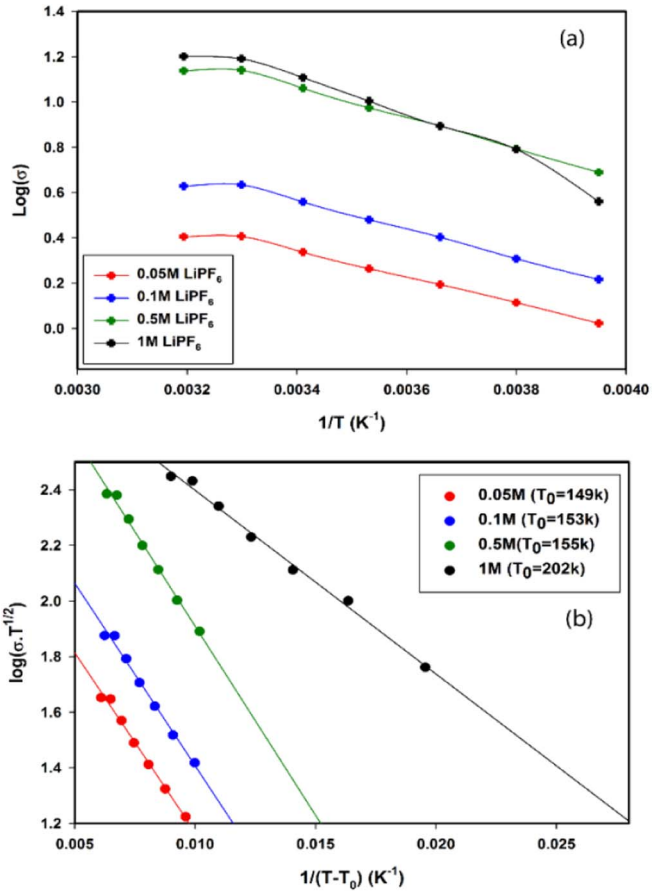

Figure 5. (a) Arrhenius plot of conductivity vs. reciprocal temperature for $LiPF_6$/DMAc at different concentrations, (b) VTF plot of conductivity-temperature data for $LiPF_6$/DMAc at different concentrations.

We know from the structural studies presented above that the Li salts form solvated ion pair complexes so that a more appropriate depiction of the conductivity versus temperature data would be by the Vogel-Tamman-Fulcher(VTF) relationship displayed in Equation 2 as previously reported.[34] The VTF ion transport mechanism has been found to explain the conductivity-temperature behavior of non- aqueous and aqueous electrolyte solutions, molten salts and polymer electrolyte systems.[34–36]

$$\text{Log}\,\sigma\,T^{1/2} = \text{Log}\,A - B/T\text{-}T_o \qquad [2]$$

In Equation 2 σ *is* conductivity, A is a pre-exponential factor proportional to $AT^{-1/2}$ and B is a constant with the dimensions of energy and is related to the critical free volume for ion transport although it is not related to any simple activation process. T_0 is the theoretical temperature at which the transport function ceases to exist or the solvent structural relaxation becomes zero.[34] It is related to the glass transition temperature (T_g) of the particular electrolyte.

The values of T_0 (Table S3) for all the solutions were obtained from the best fit of the conductivity-temperature data to the VTF equation and used to construct all of the conductivity-temperature plots in Figure 5b. The structural data presented earlier in Scheme 1 together with the linearity of the VTF plots in Figure 5b can be used to construct a depiction of the ion conduction process in DMAc electrolytes as shown in Scheme 2.

The ion movement in these electrolytes is facilitated by the mobility of the DMAc molecules. As pictured in the Scheme, movement of DMAc molecules facilitates solvated Li^+ (together with its anion pair) to make new coordination bonds with the next solvent cage allowing them to move forward to a new solvent cage.[34] The VTF ion transport mechanism depicted in Scheme 2 teaches that the movement of free solvent molecules controls the ion transport and their movement creates voids for the ions to move through.

Oxygen electrochemistry and transport studied with microelectrodes.—We have used microelectrodes to study O_2 electrochemistry in dialkylacetamide-based electrolytes because of its unique advantages in elucidating the mechanism of the ORR reactions.[12] Microelectrodes are also useful to measure O_2 transport properties such as oxygen solubility and diffusion coefficient in these electrolytes. We Provide a brief presentation of the theory of microelectrode voltammetry in the supplementary section.

Oxygen electrochemistry in DMAc.—The ORR current-voltage responses on planar carbon microelectrodes were investigated in several DMAc electrolytes containing a series of Li^+ and TBA^+ salts. The studied salts include $TBAPF_6$, $LiPF_6$, $TBACF_3SO_3$, $LiCF_3SO_3$, $TBAClO_4$, $LiClO_4$, $TBANO_3$ and $LiNO_3$. For comparison, ORR in solutions of $TBAPF_6$ and $LiPF_6$ in DMSO were also studied as well.

ORR and OER in TBA^+ salt- based DMAc electrolytes.—Figures 6 shows the voltammograms recorded on a carbon microelectrode for O_2 saturated solutions in 0.1M $TBAPF_6$/DMAc, 0.1M $TBACF_3SO_3$/DMAc, 0.1M $TBAClO_4$/DMAc, 0.1M $TBANO_3$/DMAc

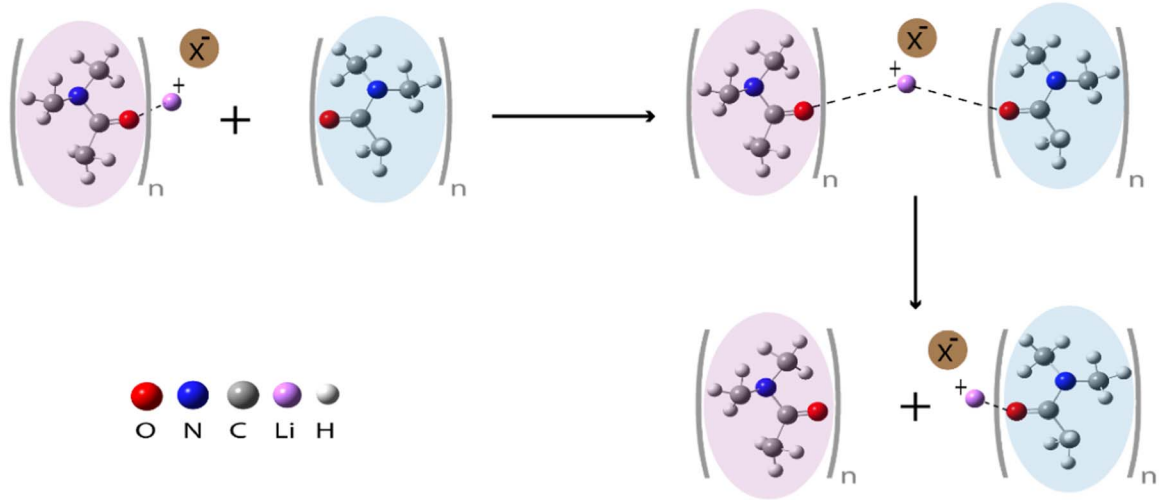

Scheme 2. Ion conductivity mechanism in DMAc-based electrolytes.

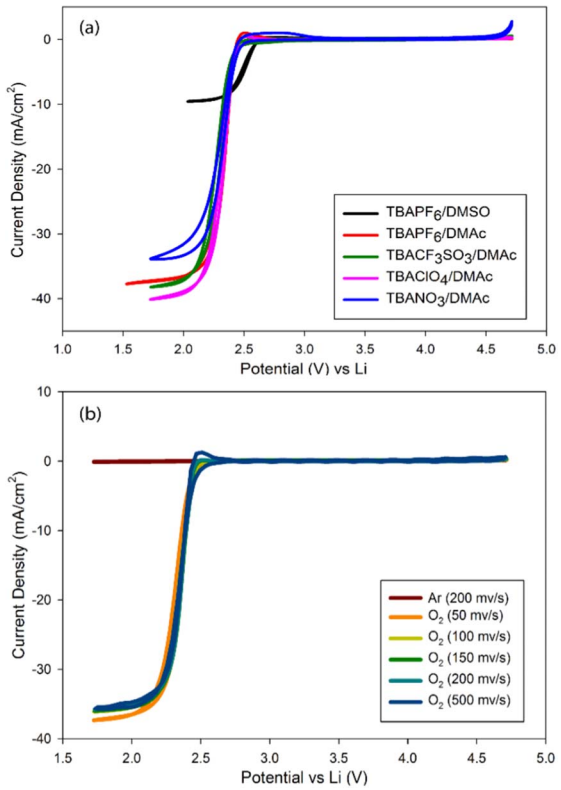

Figure 6. (a) Current-voltage response of carbon microelectrode in O_2 saturated 0.1 M of $TBAPF_6$ in DMSO and 0.1M TBA^+ salts in DMAc electrolytes at 150 mV/s scan rate. (b) Current-voltage response of carbon microelectrode in O_2 saturated 0.1M $TBAPF_6$ in DMAc electrolyte at different scan rates.

and 0.1M $TBAPF_6$/DMSO. These electrolytes exhibited the limiting current behavior as shown in Figures 8a and 8b with sigmoidal shaped current-voltage curves at scan rates ranging from 50 to 500 mV/s This behavior indicates fast O_2 transport to the electrode surface and efficient diffusion of the ORR product (superoxide, O_2^-) away from the electrode surface. We have established that this limiting current behavior on the microelectrode is due to a 1-electron ORR by measuring cyclic voltammograms of these electrolytes (see Figure 7 below) on a glassy carbon (GC) macroelectrode and analysis of the data using Randles-Sevcik relationship as previously reported.[2,8] The reversible ORR in TBA-based electrolytes is depicted in Equation 3.

$$O_2 + TBA^+ + e^- \leftrightarrows TBAO_2 \qquad [3]$$

The CV results on the GC macroelectrodes summarized in Figure 7 below will be discussed in detail later. Due to the efficient removal of O_2^- from the microelectrode surface, the return anodic sweep does not show oxidation current. Similar limiting current behavior was observed in all TBA^+-containing electrolytes indicating that the reversible electrode process is mainly controlled by the TBA^+ cation while the anions have a minimal influence on the ORR kenitics.[12] The microelectrode data also seem to indicate that the superoxide is soluble in the DMAc electrolytes. The higher ORR limiting current in DMAc electrolytes than in DMSO (Figure 6a) suggests that more O_2 is diffusing to the electrode surface. Indeed, the higher O_2 solubility and O_2^- diffusion rate measured in the DMAc electrolytes and discussed in the next section provide a rational explanation for the observed ORR behavior in these two solvents.

When a planar macroelectrode was used, the cathodic and anodic current peaks in the CV for all electrolytes had similar magnitudes (as shown in Figure 7a) indicating reversible ORR processes in all cases. However, peak separations between anodic and cathodic peaks are higher than 59 mV (Table I) due to insufficient IR correction. For the same salt, the intensity of the anodic and cathodic peaks did

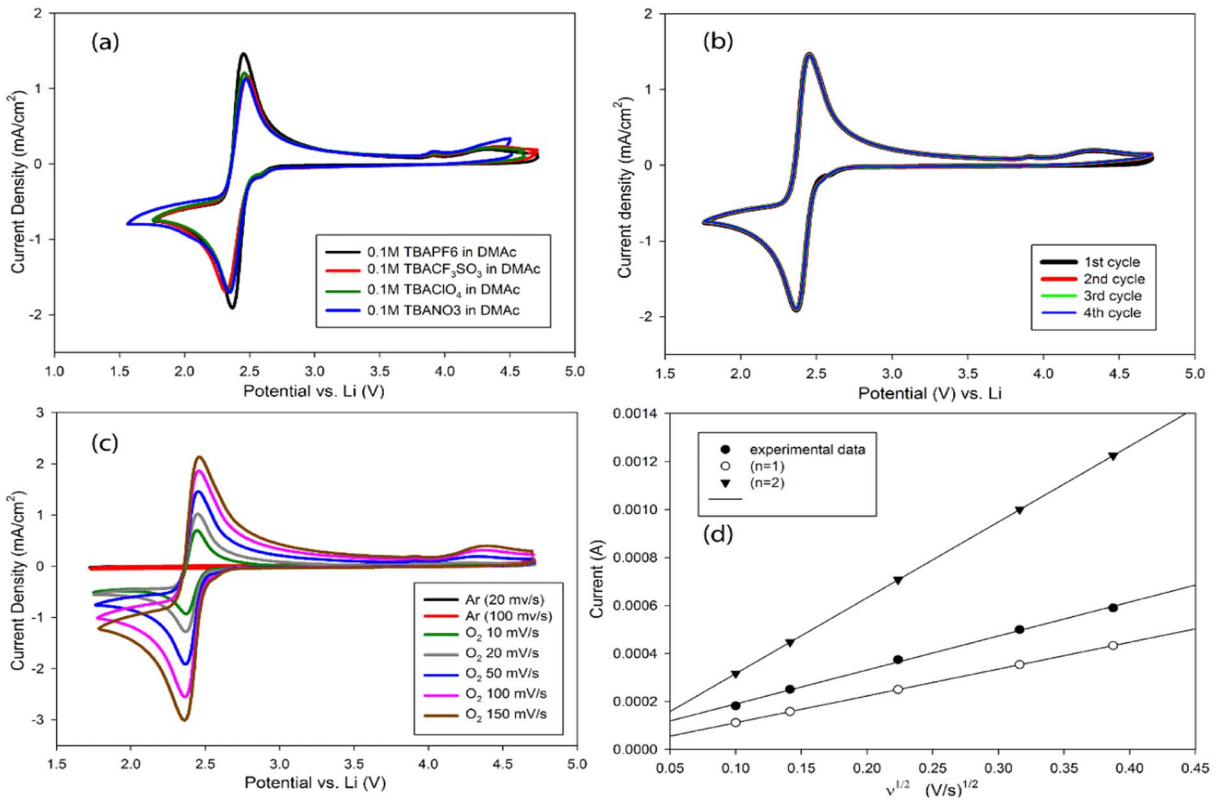

Figure 7. (a) Current-voltage response of glassy carbon macroelectrode in O_2 saturated TBA^+ electrolytes (scan rate = 50mV/s), (b) Current-voltage response of glassy carbon macroelectrode in O_2 saturated 0.1M $TBAPF_6$ in DMAc electrolyte (scan rate = 50mV/s), (c) Current-voltage response of glassy carbon macroelectrode in O_2 saturated 0.1M $TBAPF_6$ in DMAc electrolyte at different scan rates, (d) Randles-Sevcik fitting for $TBAPF_6$/DMAc.

Table I. Cyclic voltammetric data for the O_2/O_2^- redox couple in 0.1M $TBAPF_6$/DMAc.

Scan rate, ν (mV/s)	$E_{p,a}$ (V)	$E_{p,c}$ (V)	ΔE_p (V)	$E_{p,c/2}$ (V)	No. of e- (n)
10	2.4437	2.3717	0.072	2.435	0.892575
20	2.4488	2.37	0.0788	2.4374	0.838279
50	2.4535	2.365	0.0885	2.4382	0.771858
100	2.4572	2.3659	0.0913	2.4411	0.75133
150	2.4561	2.3624	0.0937	2.4391	0.736636

not reduce with the cycling in all the DMAc electrolytes indicating good reversibility of this system (Figure 7b). Moreover, increasing the scan rate increased the anodic and cathodic peak hight in the same magnitude which is a characteristic of a reversible process as well (Figure 7c). These observations support the microelectrode results. The ORR process was found to be a one-electron process in all the electrolytes as determined from the analysis of the data using Randles-Sevcik equation as done previously.[2,3,12]

$$I_{pa} = \left(2.69 \times 10^5\right) n^{3/2} A D^{1/2} V^{1/2} C \quad [4]$$

Figure 7d depicts the Randles-Sevcik plots for ORR in the $TBAPF_6$/DMAc electrolyte. In all electrolytes, the slope of the experimental i vs $v^{1/2}$ is a better fit for a one-electron process more than the two-electron process. Both the microelectrode and macroelectrode data support the view that the ORR in these electrolytes is governed by the hard-soft acid base theory. The soft TBA^+ Lewis acid[1] interacts strongly with the soft Lewis base O_2^- to form the soluble $TBAO_2$ ion pair. The interaction between TBA^+ and O_2^- is strong enough to prevent O_2^- from further reduction to form the peroxide.[1–3] The O_2 voltammetry data in the various electrolytes indicate that TBA^+ cation primarily controls the electrode process while the anions have a very minor, if any, influence on the ORR mechanism.[1]

Table I displays the number of electrons involved in the ORR calculated from the voltammetric data in Figure 7c for the O_2/O_2^- redox couple in 0.1M $TBAPF_6$/DMAc. The number of electrons (n) transferred in the reaction was calculated from Equation 5:

$$E_{p/2} - E_p = 2.2\ (RT/nF) \quad [5]$$

where $E_{p/2}$ is the half-peak potential at the half value of the peak current, E_p is the peak potential, n is the number of electrons involved in the reaction and F is Faraday constant.[2] The number of electrons calculated was close to 1 in all tested electrolytes. Similar values were calculated for the other electrolytes as well.

O_2 transport properties.—Oxygen solubility and diffusion coefficients were calculated from the Cottrell plots (Figure 8) derived from chronoamperometry measurements in the various electrolytes conducted using the microelectrode (Table II), as we reported previously.[12] The oxygen solubility and diffusion coefficient in $TBAPF_6$/DMAc were found to be 3.09×10^{-6} mol/cm^{-3} and 5.09×10^{-5} cm^2 s^{-1}, respectively. The oxygen solubility and permeability for all the TBA^+/DMAc electrolytes are higher than those in the $TBAPF_6$/DMSO while the oxygen diffusion coefficients are similar. Furthermore, these values in $TBANO_3$/DMAc electrolyte are comparable to the other TBA^+/DMAc electrolytes. These findings are

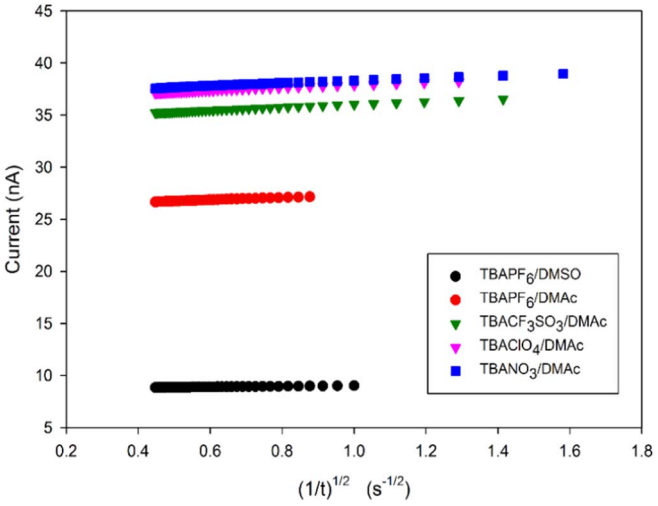

Figure 8. Cottrell plots derived from chronoamperometry measurements made with the microelectrode in different 0.1M TBA^+ salts in DMAc and DMSO solvents.

in agreement with the physical properties we have measured for the electrolytes (Table S1). Superoxide (O_2^-) diffusion coefficient values were calculated using Equation 6, where n is the number of electrons involved in the formation of O_2^-, E^0 is the standard potential, $E_{1/2}$ is the half wave potential, R is the gas constant, T is the temperature in Kelvin, F is Faraday's constant, D_o is the diffusion coefficient of the oxidized species (oxygen) and D_R is the diffusion coefficient of the reduced species (superoxide).[12]

$$n\left(E^0 - E_{1/2}\right) = (RT/F)\ln\left(D_o/D_R\right) \quad [6]$$

The E^0 values were found for each electrolyte from the average of onset potentials at different scan rates using the microelectrode. The superoxide diffusion rates in the DMAc electrolytes are comparable to those in $LiPF_6$ in DMSO (Table II). Its value for 0.1M $LiPF_6$ in DMAc was a bit higher than that for 0.1M $LiPF_6$ in DMSO suggesting that the superoxide diffusion away from the electrode surface in $LiPF_6$/DMAc is slightly faster than that in $LiPF_6$/DMSO.

ORR and OER in Li^+ salt- based DMAc electrolytes.—Oxygen reduction reactions on microelectrodes exhibited a distinctly different current-voltage behavior in lithium salt-based electrolytes than that observed in the TBA^+-containing electrolytes discussed above. Figure 9 displays the voltammograms recorded for O_2 saturated solutions of 0.1M $LiPF_6$/DMAc, 0.1M $LiCF_3SO_3$/DMAc, 0.1M $LiClO_4$/DMAc and 0.1M $LiNO_3$/DMAc. These voltammograms do not show a limiting current. Instead, a cathodic peak is observed at all applied scan rates in these electrolytes. Such current-voltage profile on a microelectrode is indicative of an irreversible ORR process. The causes as we mentioned in the supporting information section include: deposition of insoluble reduction products on the electrode surface; the occurrence of a second reaction where the negatively charged products of the first reaction is further reduced and as the potential of the microelectrode becomes more negative to the zero charge, the

Table II. Oxygen mass transport parameters in 0.1M TBA^+ salt electrolytes in DMAc and DMSO.

Electrolyte	Oxygen Solubility (mol./cm^3)	Oxygen Diffusion Coefficient (cm^2/s)	Oxygen Permeability (mol/cm.s)	i_l (A)	E^0 (V)	$E_{1/2}$ (V)	Superoxide Diffusion Coefficient (cm^2/s)
PF_6^-/ DMSO	7.09×10^{-7}	7.38×10^{-5}	5.23×10^{-11}	1.11×10^{-8}	2.60	2.48	6.89×10^{-7}
PF_6^-/ DMAc	3.09×10^{-6}	5.09×10^{-5}	1.57×10^{-10}	3.34×10^{-8}	2.44	2.34	1.04×10^{-6}
$CF_3SO_3^-$/DMAc	3.33×10^{-6}	6.23×10^{-5}	2.07×10^{-10}	4.41×10^{-8}	2.39	2.26	3.94×10^{-7}
ClO_4^-/DMAc	2.97×10^{-6}	7.37×10^{-5}	2.19×10^{-10}	4.65×10^{-8}	2.42	2.30	6.89×10^{-7}
NO_3^-/DMAc	2.67×10^{-6}	8.31×10^{-5}	2.22×10^{-10}	4.71×10^{-8}	2.43	2.30	5.26×10^{-7}

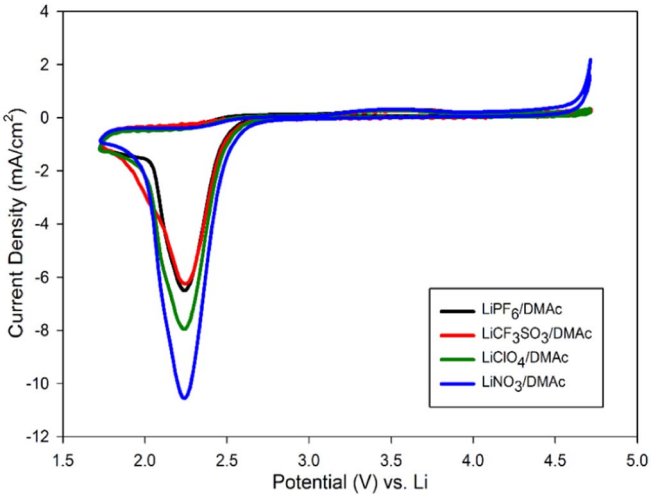

Figure 9. Current-voltage response of carbon microelectrode in O_2 saturated 0.1M Li^+ salt electrolytes (scan rate = 150mV/s).

negatively charged species are repulsed away and depleted from the electrode surface reducing the number of reactants available for the second reaction.[37] The well-recognized sequential reduction of O_2 to O_2^- and O_2^{2-} in Li^+-containing electrolytes depicted in Equations 7 and 8 would exemplify this:

$$O_2 + Li^+ + e^- \rightarrow LiO_2 \quad [7]$$

$$LiO_2 + Li^+ + e^- \rightarrow Li_2O_2 \quad [8]$$

Identifying the microelectrode current-potential profile in Li^+-conducting electrolytes.—In order to distinguish between multiple causes for the peak shape of the i-V profile on the microelectrode, several experiments were conducted.

First we performed ORR in the same electrolytes on macro-electrodes with a view to analyze the data using the well-known Nicholoson-Shain relationship[2] applicable to irreversible processes, and calculate the number of electrons involved in the ORR reaction.

Figure 10a displays the voltammograms recorded on the planar GC macroelectrode in O_2 saturated solutions of 0.1M $LiPF_6$/DMAc, 0.1M $LiCF_3SO_3$/DMAc 0.1M $LiClO_4$/DMAc and 0.1M $LiNO_3$/DMAc. Clearly, irreversible ORR with anodic current peaks much smaller than the cathodic peaks is observed in all electrolytes These observations obtained using the micro- and macro- electrodes are in agreement with previous studies showing that ORR tend to become less reversible in the presence of small hard Lewis acid cations such as Li^+.[2,3] The multiple anodic peaks versus a single cathodic peak suggests that the cathodic electrochemical process is probably accompanied by chemical steps producing multiple products that are subsequently oxidized as we previously discussed for ORR in DMSO.[38] The reduction peak

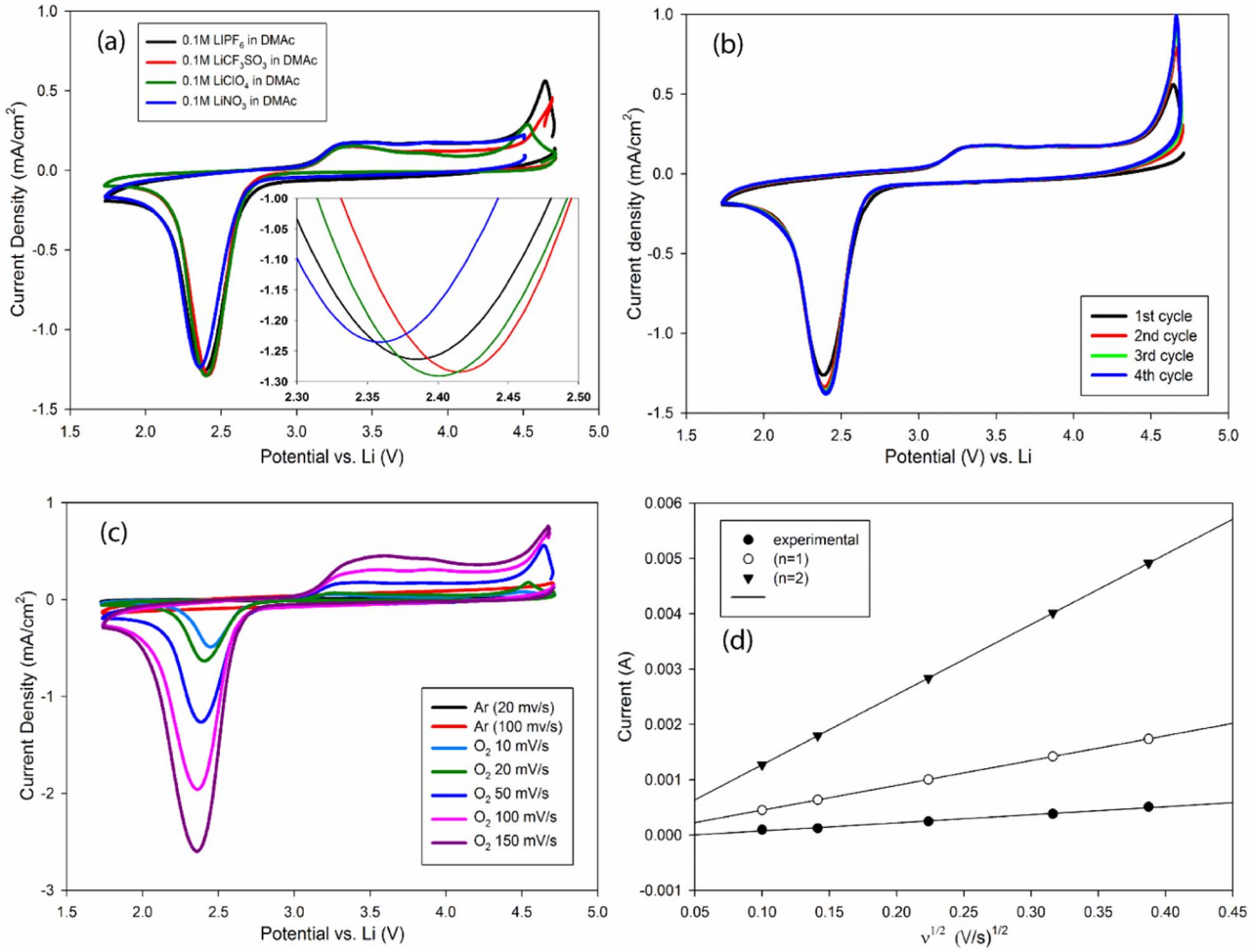

Figure 10. (a) Current-voltage response of glassy carbon macroelectrode in O_2 saturated Li^+ electrolytes (scan rate = 50mV/s), (b) Current-voltage response of glassy carbon macroelectrode in O_2 saturated 0.1M $LiPF_6$ in DMAc (scan rate = 50mV/s), (C) Current-voltage response of glassy carbon macroelectrode in O_2 saturated 0.1M $LiPF_6$ in DMAc at different scan rates, (d) Nicholson-Shain plots for ORR in $LiPF_6$/DMAc.

position of triflate was very slightly shifted to lower values than those of the other electrolytes (Figure 10a inset). This is attributed to the stronger interaction between lithium triflate and DMAc than the other lithium salt electrolytes (due to a direct interaction between the Li^+ ion and the triflate ion based on the FTIR and NMR studies presented above). The order of the shift in the reduction peak follows the same trend observed in the ^{13}C NMR for the C=O group ($NO_3^- < ClO_4^- < PF_6^- < CF_3SO_3^-$) approximately following order of electron donating property of the anion. In all Li^+/DMAc electrolytes, the intensity of the cathodic and anodic peaks was not affected by the number of cycles suggesting that the ORR process is chemically reversible but kinetically irreversible (Figure 10b) similar to the behavior of Li^+/DMSO electrolytes.[2,3,12] It is also observed that when the scan rate was increased, the peak intensity increased as well (Figure 10c).

The ORR peak was analyzed using the Nicholson-Shain equation which relates the peak current to the square root of the sweep rate for irreversible reactions according to Equation 9. The number of electrons involved in the oxygen reduction reaction can be calculated from the slope of the plots of I_p versus $V^{1/2}$.[2,3]

$$I_p = \left(2.99 \times 10^5\right) n\,(n\alpha)^{1/2}\,ACD^{1/2}\,V^{1/2} \qquad [9]$$

Figure 10d shows a plot of the experimental CV peak current intensities at different sweep rates in the 0.1M $LiPF_6$/DMAc electrolyte fitted to the Nicholson-Shain equation together with theoretical plots obtained for n = 1 and 2. Similar fitting was done for the other electrolytes as well. The slopes for the experimental data agreed with a one-electron process better than a two-electron process. This one electron process could be the reduction of O_2 to superoxide as depicted in Equation 7 or to the reduction of LiO_2 to Li_2O_2 as in Equation 8. In presence of Li salts the superoxide will decompose to Li_2O_2 and O_2 as shown below.

$$2\,LiO_2 \rightarrow Li_2O_2 + O_2 \qquad [10]$$

To gain further insights into the ORR mechanism in Li^+/DMAc electrolytes, the cathodic scan was reversed at different potentials and the anodic current-potential behavior was examined after each potential reversal. Figure 11a shows the related CVs recorded in 0.1M $LiPF_6$/DMSO while Figure 11b shows the related CVs recorded in 0.1M $LiPF_6$/DMAc. For potentials reversed before the cathodic peak at 2.4V an anodic peak was observed around 2.9V which was not seen when the cathodic scan was reversed at or below the cathodic peak potential of 2.4V. As we reported previously for ORR in Li^+/DMSO electrolytes,[38] this anodic peak at 2.9 V is most probably due to the oxidation of superoxide formed as the initial reduction product of O_2 in the downward sloping potential region of the cathodic sweep in Figure 11b (see Equation 7).[3,12] Zhang et al. has assigned this peak to the oxidation of the adsorbed state of O_2^- (initially formed by reduction of O_2).[23] When the potential is reversed at the cathodic peak potential of 2.4V, the anodic peak at 2.9V is absent; instead, a broad peak at 3.4V emerges. This is most likely due to the oxidation of the Li_2O_2 formed from the decomposition or reduction of LiO_2 to Li_2O_2 at potentials near the cathode peak at 2.4V. According to Zhang et al., this peak is assigned to the oxidation of a mixture of LiO_2 and Li_2O_2.[23] Since the Nicholson-Shain analysis was done for the currents at the cathodic peak potential, it is reasonable to conclude that the one-electron reaction revealed by the plot in Figure 11 conforms to the reduction of superoxide to peroxide as shown in Equation 8. The anodic peaks' intensities in DMAc are much lower than those in DMSO compared to the cathodic peak which indicates lower availability of the ORR intermediates on the electrode surface. This means that the diffusion of O_2^- from the electrode surface in DMAc is faster (in agreement with the calculated diffusion coefficient values of O_2^-).

We carried out a second experiment to identify whether the peak shape of the voltammogram on the microelectrode in Li^+-containing electrolytes was caused by the deposition of insoluble products on the electrode surface or the repulsion between the charged species O_2^- and O_2^{2-} at the electrode surface. This involved running a CV on the microelectrode in a Li^+ electrolyte first and then using the same electrode containing any insoluble ORR products deposited on

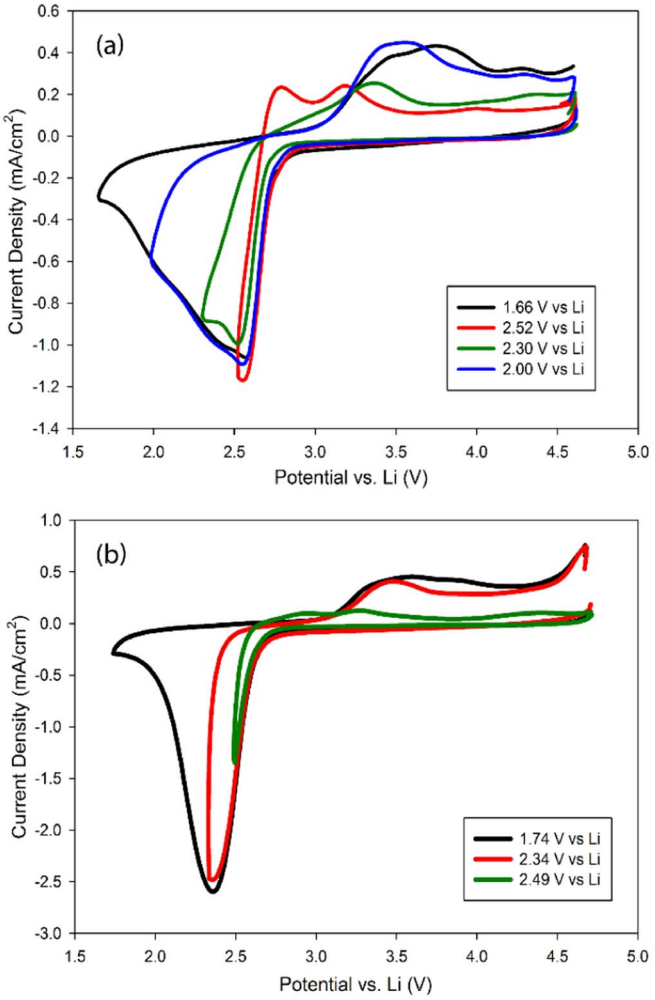

Figure 11. Current-voltage response of glassy carbon macroelectrode reversed at different potentials (scan rate = 100 mV/s): (a) $LiPF_6$/DMSO, (b) $LiPF_6$/DMAc.

it to acquire a CV in the corresponding TBA^+ electrolyte. Figure 12 shows that for ORR in $LiPF_6$ electrolyte the peak on the microelectrode voltammogram is caused mainly by the deposition of insoluble reduction products on the electrode surface. This leads to the formation of a passivating film as the current intensity on the electrode transferred from the Li^+ containing is significantly lower.

Oxygen electrochemistry in DEAc.—We carried out a limited amount of microelectrode voltammetry studies in $TBAPF_6$ and $LiPF_6$ electrolytes in diethylactemaide, (($CH_3CON(C_2H_5)_2$ DEAc) in order to assess how they compare with those in DMAc. Figure 13a clearly shows that the ORR process on the microelectrode in the DEAc electrolyte is a reversible process, similar to DMAc electrolytes, and that the limiting current is higher than in both DMSO and DMAc based electrolytes indicating that more O_2 is being reduced. The onset potential is higher than in DMSO which is higher than that of DMAc as well. The trend of the onset potential for the reduction of O_2 to O_2^- seems to follow the solvent Donor Number in the order DEAc>DMSO>DMAc. The sigmoidal shape is maintained for 0.1M $TBAPF_6$/DEAc at different scan rates indicating a reversible process (Figure 13b). Cottrell plot for $TBAPF_6$/DEAc (Figure 13c) had higher currents than those for DMAc and DMSO. Oxygen mass transport parameters calculated from the Cottrell plots gave O_2 solubility of 5.31×10^{-6} mol/cm^{-3}, diffusion coefficient of 6.77×10^{-5} cm^{2}s^{-1}, permeability of 3.59×10^{-11} mol/cm.s, and superoxide diffusion coefficient of 1.33×10^{-7} cm^{2}s^{-1}. The O_2 solubility is higher

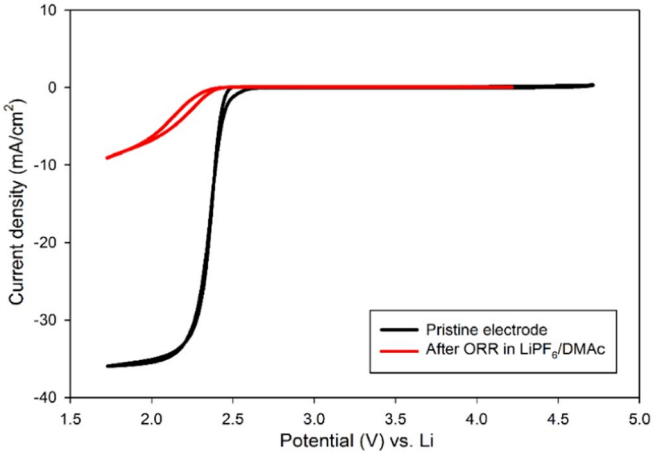

Figure 12. Current-voltage response for ORR in (0.1M) $TBAPF_6$/DMAc in exclusion experiments on carbon microelectrode.

than in DMAc and DMSO electrolytes. That explains the higher O_2 limiting current observed on the microelectrode in DEAc/$TBAPF_6$ and the smaller overpotential needed to start the ORR process. The oxygen diffusion coefficients for DMAc and DEAc were comparable while the superoxide diffusion coefficients were lower in DEAc electrolytes.

When the planner macroelectrode was used in argon saturated $TBAPF_6$/DEAc electrolyte (Figure 13d), the scans showed a reaction at 2 V which was not present in the case of DMAc electrolytes (most likely it is due to the reduction of the DEAc solvent). While in the presence of oxygen, only a cathodic peak was observed at all scan rates (no anodic peak) indicating that the reduction products (superoxide) were no longer available for the oxidation process on the electrode surface. The exact cause of this is not known at this time.

The ORR behavior in Li^+/DEAc was somewhat different from what it was in the DMSO and DMAc electrolytes. The ORR current-voltage responses on the microelectrode in DEAc electrolyte show some reversibility as indicated by the absence of an anodic peak. However, there was a small cathodic current peak at about 2.2 V before the current seemingly approaches a steady state profile (Figure 14a). This seems to suggest some irreversibility in the reduction process probably as a result of the ORR possibly involving two closely lying processes. When the CV was run on a planar macroelectrode in O_2 saturated 0.1M $LiPF_6$/DEAc electrolyte, only a cathodic peak was observed between 1.8 and 4.0V at all scan rates (Figure 14b). This observation is in agreement with that found in the TBA^+/DEAc electrolyte indicating that this behavior is not caused by the cation species but probably associated with the reduction of the solvent.

Conclusions

We have found that lithium salts form solvates of the structures, $Li^+[O{=}C(CH_3)(N(CH_3)_2]_n\ X^-$ in DMAc and DEAc in which an

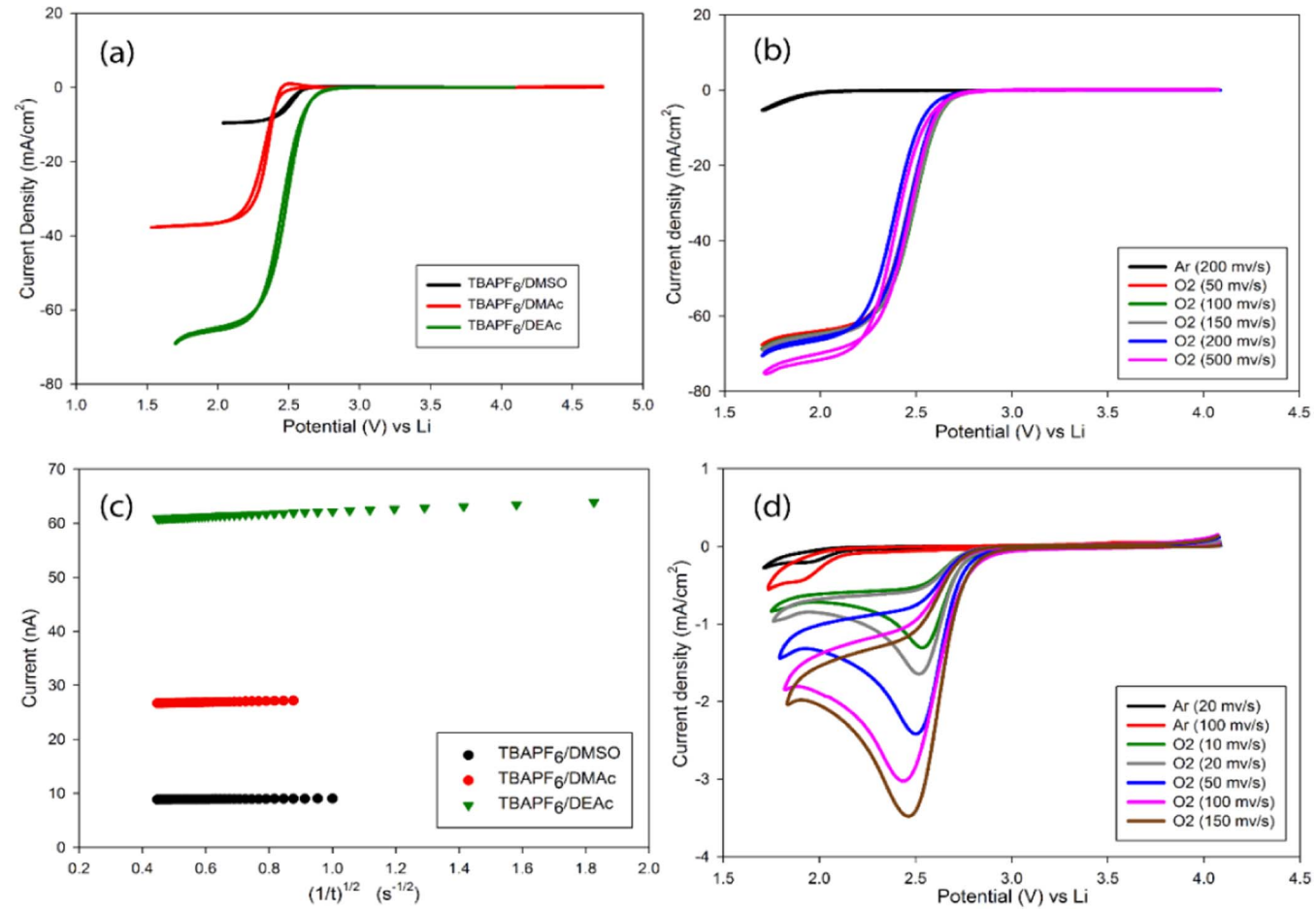

Figure 13. (a) Current-voltage response of carbon microelectrode in O_2 saturated 0.1M $TBAPF_6$ electrolytes in 3 different solvents (DMSO, DMAc and DEAc) (scan rate = 150mV/s), (b) Current-voltage response of carbon microelectrode in O_2 saturated 0.1M $TBAPF_6$/DEAc electrolyte at different scan rates, (c) Cottrell plots derived from chronoamperometry measurements made with the microelectrode in different $TBAPF_6$ salts in DMAc, DEAc and DMSO solvents, (d) Current-voltage response of planner glassy carbon macroelectrode in 0.1M $TBAPF_6$/DEAc electrolyte at different scan rates.

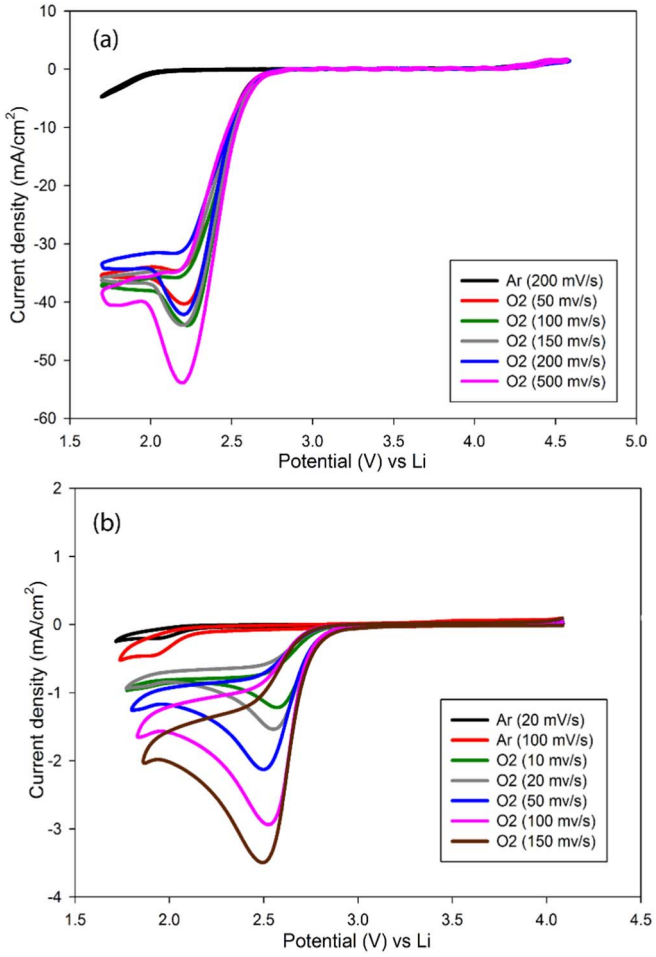

Figure 14. (a) Current-voltage response of carbon microelectrode in 0.1M $LiPF_6$/DEAc at different scan rates, (b) Current-voltage response of planner glassy carbon macroelectrode in 0.1M $LiPF_6$/DEAc electrolyte at different scan rates.

electron donor bond is formed between the carbonyl oxygen of the amide and Li^+. Our FT-IR and NMR data lead us to conclude that for Li^+ salt solutions in high DN solvents, the type of ion pair formed is not affected by the DN of the counter anion but rather by its size. Among the counter anions studied, only the triflate showed FT-IR shifts indicating the formation of contact ion pairs of the structure $(CF_3SO_3^-Li^+(DMAc)_3$. On the other hand, TBA^+ cations did not appear to form such solvation bonds with the amides. It appears that the relatively good solubility of TBA^+ salts in the amide solvents results from dipolar interactions. The ORR in solutions of TBA^+ salts in the dialkylacetamides showed a reversible one-electron process with the formation of stable $TBAO_2$. This property allowed us to determine oxygen solubility, diffusion coefficient and permeability, and superoxide diffusion coefficient in the dialkylacetamide electrolytes. The ORR in all Li^+ salt solutions studied on macro and microelectrodes revealed that the multi-electron reduction of O_2 although chemically reversible is kinetically irreversible.

Acknowledgments

The financial support from the U.S. Army CERDEC provided through subcontract No. GTS-S-15-015 is acknowledged. We thank Professor Jason J. Guo for performing ^{15}N NMR experiments.

ORCID

K. M. Abraham https://orcid.org/0000-0002-1790-1775

References

1. C. J. Allen, J. Hwang, R. Kautz, S. Mukerjee, E. J. Plichta, M. A. Hendrickson, and K. M. Abraham, *The Journal of Physical Chemistry C*, **116**, 20755 (2012).
2. C. O. Laoire, S. Mukerjee, K. M. Abraham, E. J. Plichta, and M. A. Hendrickson, *The Journal of Physical Chemistry C*, **113**, 20127 (2009).
3. C. O. Laoire, S. Mukerjee, K. M. Abraham, E. J. Plichta, and M. A. Hendrickson, *The Journal of Physical Chemistry C*, **114**, 9178 (2010).
4. J. M. Alía and H. G. Edwards, *Vibrational Spectroscopy*, **24**, 185 (2000).
5. D. G. Kwabi, V. S. Bryantsev, T. P. Batcho, D. M. Itkis, C. V. Thompson, and Y. Shao-Horn, *Angewandte Chemie*, **128**, 3181 (2016).
6. X. Xuan, J. Wang, Y. Zhao, and J. Zhu, *Journal of Raman Spectroscopy: An International Journal for Original Work in all Aspects of Raman Spectroscopy, Including Higher Order Processes, and also Brillouin and Rayleigh Scattering*, **38**, 865 (2007).
7. Y. Yamada, Y. Takazawa, K. Miyazaki, and T. Abe, *The Journal of Physical Chemistry C*, **114**, 11680 (2010).
8. K. M. Abraham, *Journal of The Electrochemical Society*, **162**, A3021 (2015).
9. C. M. Burke, *Electrolyte Engineering to Improve Capacity and Rechargeablility in the Lithium-Oxygen Battery*, in, UC Berkeley (2018).
10. C. M. Burke, V. Pande, A. Khetan, V. Viswanathan, and B. D. McCloskey, *Proceedings of the National Academy of Sciences*, **112**, 9293 (2015).
11. G. A. Elia, J. B. Park, Y. K. Sun, B. Scrosati, and J. Hassoun, *ChemElectroChem*, **1**, 47 (2014).
12. I. Gunasekara, S. Mukerjee, E. J. Plichta, M. A. Hendrickson, and K. M. Abraham, *Journal of The Electrochemical Society*, **161**, A381 (2014).
13. I. Gunasekara, S. Mukerjee, E. J. Plichta, M. A. Hendrickson, and K. M. Abraham, *Journal of The Electrochemical Society*, **162**, A1055 (2015).
14. G. Horwitz, M. Factorovich, J. Rodriguez, D. Laria, and H. R. Corti, *ACS Omega*, **3**, 11205 (2018).
15. L. Johnson, C. Li, Z. Liu, Y. Chen, S. A. Freunberger, P. C. Ashok, B. B. Praveen, K. Dholakia, J.-M. Tarascon, and P. G. Bruce, *Nature chemistry*, **6**, 1091 (2014).
16. H.-M. Kwon, M. L. Thomas, R. Tatara, A. Nakanishi, K. Dokko, and M. Watanabe, *Chemistry Letters*, **46**, 573 (2017).
17. B. D. McCloskey, D. S. Bethune, R. M. Shelby, G. Girishkumar, and A. C. Luntz, *The Journal of Physical Chemistry Letters*, **2**, 1161 (2011).
18. D. Sharon, D. Hirsberg, M. Salama, M. Afri, A. A. Frimer, M. Noked, W. Kwak, Y.-K. Sun, and D. Aurbach, *ACS applied materials & interfaces*, **8**, 5300 (2016).
19. R. Tatara, D. G. Kwabi, T. P. Batcho, M. Tulodziecki, K. Watanabe, H.-M. Kwon, M. L. Thomas, K. Ueno, C. V. Thompson, and K. Dokko, *The Journal of Physical Chemistry C*, **121**, 9162 (2017).
20. A. von Wald Cresce, O. Borodin, and K. Xu, *The Journal of Physical Chemistry C*, **116**, 26111 (2012).
21. Y. Wang, N.-C. Lai, Y.-R. Lu, Y. Zhou, C.-L. Dong, and Y.-C. Lu, *Joule*, **2**, 2364 (2018).
22. K. Xu, *Chemical reviews*, **104**, 4303 (2004).
23. Y. Zhang, X. Zhang, J. Wang, W. C. McKee, Y. Xu, and Z. Peng, *The Journal of Physical Chemistry C*, **120**, 3690 (2016).
24. D. G. Kwabi, T. P. Batcho, S. Feng, L. Giordano, C. V. Thompson, and Y. Shao-Horn, *Physical Chemistry Chemical Physics*, **18**, 24944 (2016).
25. W. Walker, V. Giordani, J. Uddin, V. S. Bryantsev, G. V. Chase, and D. Addison, *Journal of the American Chemical Society*, **135**, 2076 (2013).
26. V. Giordani, W. Walker, V. S. Bryantsev, J. Uddin, G. V. Chase, and D. Addison, *Journal of The Electrochemical Society*, **160**, A1544 (2013).
27. J. Uddin, V. S. Bryantsev, V. Giordani, W. Walker, G. V. Chase, and D. Addison, *J. Phys Chem Lett.*, **4**, 3760 (2013).
28. K. M. Abraham, R. Rauh, and S. Brummer, *Electrochimica Acta*, **23**, 501 (1978).
29. A. J. Wain, G. G. Wildgoose, C. G. Heald, L. Jiang, T. G. Jones, and R. G. Compton, *The Journal of Physical Chemistry B*, **109**, 3971 (2005).
30. D. H. Johnston and D. F. Shriver, *Inorganic Chemistry*, **32**, 1045 (1993).
31. J. Alía, Y. Díaz, H. Edwards, F. García, and E. Lawson, *Journal of molecular structure*, **408**, 439 (1997).
32. S. A. Suthanthiraraj, R. Kumar, and B. J. Paul, *Spectrochimica Acta Part A: Molecular and Biomolecular Spectroscopy*, **71**, 2012 (2009).
33. M. Schmeisser, P. Illner, R. Puchta, A. Zahl, and R. van Eldik, *Chemistry–A European Journal*, **18**, 10969 (2012).
34. G. Gu, R. Laura, and K. M. Abraham, *Electrochemical and solid-state letters*, **2**, 486 (1999).
35. G. Adam and J. H. Gibbs, *The journal of chemical physics*, **43**, 139 (1965).
36. M. H. Cohen and D. Turnbull, *The Journal of Chemical Physics*, **31**, 1164 (1959).
37. J. D. Norton, H. S. White, and S. W. Feldberg, *Journal of physical chemistry*, **94**, 6772 (1990).
38. M. J. Trahan, S. Mukerjee, E. J. Plichta, M. A. Hendrickson, and K. M. Abraham, *Journal of The Electrochemical Society*, **160**, A259 (2013).